A New Clutter Elimination and Downrange Correction Algorithm for Through Wall Radar Detection

Dheyaa T. Al-Zuhairi[*]**, Abbas Salman Hameed, and Sura F. Yousif**

Abstract—Through wall radar imaging and detection applications are growing significantly. However, the target response is usually accompanied with a strong clutter which veils the target detection. In this paper, a new algorithm is proposed for clutter reduction and target downrange correction in through wall monostatic radar imaging. The proposed algorithm arranges the received radar signals in a matrix and then splits this matrix to frames. The frames are individually processed and filtered in frequency domain, then they are returned to time domain and merged together in a new matrix. The final step is enhancing the target response via a matched filter. The proposed algorithm performance is evaluated by target to clutter ratio (TCR), signal to clutter ratio (SCR), and downrange target position error (DTPE) in three different simulated scenarios. The simulation results exhibit the proposed algorithm capability in both removing the clutter and adjusting the target downrange to be with an evident appearance and accurate position. In the most complicated scenario which consists of two separated walls and a target behind them, using the proposed algorithm improves the performance in terms of TCR, SCR, and DTPE by 49.7 dB, 70.7 dB, and 7.6%, respectively.

1. INTRODUCTION

The growth of services presented by Through Wall Imaging (TWI) for humanity in important fields, which include security, surveillance, fire-fighting, hostages saving, suspects tracking, and elders monitoring, has significantly motivated the scientific research in this area [1–3].

One of the most familiar approaches in TWI is Ultra-Wideband (UWB) radar technique [4, 5]. The short-time pulses adopted by this technique support high resolution resolving adjacent targets [5, 6]. In radar TWI, the transmitter illuminates the desired region by electromagnetic waves. Due to the differences in the dielectric properties of the objects on the transmission broadside, the traveling waves are scattered and reflected [6, 7]. The reflected waves are utilized to detect the targets behind walls. However, the target response is usually contaminated and covered by strong clutter produced from the antenna self-reflection and reflected waves from the surrounding walls [1, 8].

The simplest clutter removing method is the background subtraction in which the clutter is removed by subtracting the data of the scenario without the target from the scenario data with the target. Nevertheless, the no-target background data is not usually available in practice [9]. Averaging is a well-known basic clutter removing approach in TWI [10]. In this approach the clutter is mitigated by subtracting the average of all the radar signals from the signal which needs to be clutter-free [10]. However, this method usually leads to attenuating the target response in the radar signals. The stationary clutter can be mitigated by the moving average window (MAW) method where the clutter in every data sample is estimated from averaging data samples in a moving window [11]. The drawback of the moving average filter is its frequency characteristics represented by the high filter ripples and poor frequency bands separation.

The researchers in [12] studied the factor analysis method and eigenvalues decomposition techniques including PCA, ICA, and SVD for clutter reduction in TWI. The results show the superiority of ICA technique in target detection over the other techniques. A radiation pattern-based Delay-Sum algorithm performance in through wall clutter reduction is compared with the conventional Delay-Sum algorithm in [13]. The comparison is based on measuring the target to clutter ratio, and it is found that the radiation pattern-based approach overcomes the conventional one [13]. However, the researchers did not consider the difference in the traveling wave speed between the walls and free space, and consequently the detection was with a wrong downrange. Another approach for through wall clutter mitigation is introduced in [8].

In this approach, SVD is utilized to separate the signals into wall and target subspaces. Then the subspace orthogonal to the wall subspace is chosen to remove clutter produced by the wall reflection from the radar signals [8]. The SVD algorithm is adopted in [14] also to separate the clutter from the target response in the radar signals.

In [15], a method based on low-rank (LR) and sparsity is developed to reduce in-wall clutter for radar objects detection. Like [15], the researchers in [16, 17] used LR matrix completion and LR auto-encoder to eliminate the clutter in sparse represented radar imaging. In [18], a weighted nuclear norm minimization is utilized to remove clutter in sparse representation of radar signals. However, these methods require an iterative algorithm for optimization, which is usually a time consuming process.

Vishwakarma and Ram proposed a neural network to decrease the dimensionality and consequently get rid of clutter in through wall radar detection [19]. The optimization process time is shortened by implementing machine learning paths multipliers via alternating direction instead of backpropagation methods. In [20], the SVD approach is developed and applied in pseudo-random continuous wave radar. In that method, the wall clutter is eliminated by identifying the position of the peak after signals subspace correlation. Variety of filters are also incorporated in removing clutter from through wall radar signals [21–23].

In this paper, a new algorithm is proposed to eliminate clutter from radar signals used in through wall radar imaging. The clutter-free signals processed by the proposed method are ready to be utilized by any imaging algorithm to produce radar focused images. The main contribution of this work is summarized in the following few rows. The A-scan radar signals are merged in a matrix which is divided later into frames called frame matrices. Each frame matrix, which includes a synchronous portion of all the radar signals, is processed individually. By measuring the signals' similarity value within each frame, then comparing this value with a threshold, a decision is made to determine whether the processed portion comes from the target or a clutter source. After converting the frame data to the frequency domain, a filter is exploited to remove the clutter. The filter output is returned to the time domain, then all the frames are collected together to form a clutter-removed matrix. As a final step, the target response is boosted by utilizing a matched filter. Another contribution besides the clutter elimination is that the proposed algorithm can correct the target downrange error caused by walls existence in the propagated signals path. The downrange correction depends on the estimation of walls material and thickness and considering their values in the calculation.

At the end of the introduction section, the paper organization map is arranged according to the following. Section 2 illustrates the clutter problem in TWI. The design of the filter on which the proposed clutter removal depends is presented in Section 3, while Section 4 describes the entire proposed clutter elimination algorithm. The simulation and results are presented and discussed in Section 5. Finally, the main points of the conclusions are summarized in Section 6.

2. CLUTTER PROBLEM IN THROUGH WALL DETECTION

In TWI using radar technique, the radar sends short pulses via the transmitting antenna. The transmitted signal is scattered by the objects in the region, and the reflected signal is captured by the receiving antenna. The reflected signals are collected at different antenna positions to be processed for image creation. Either monostatic, bi-static, or multi-static radar approach can be used for signal transmitting and echo collection [6].

Unfortunately, the target response in the collected signals is very weak compared to the clutter. In monostatic approach, clutter usually comes from the antenna self-reflection and the reflections from the
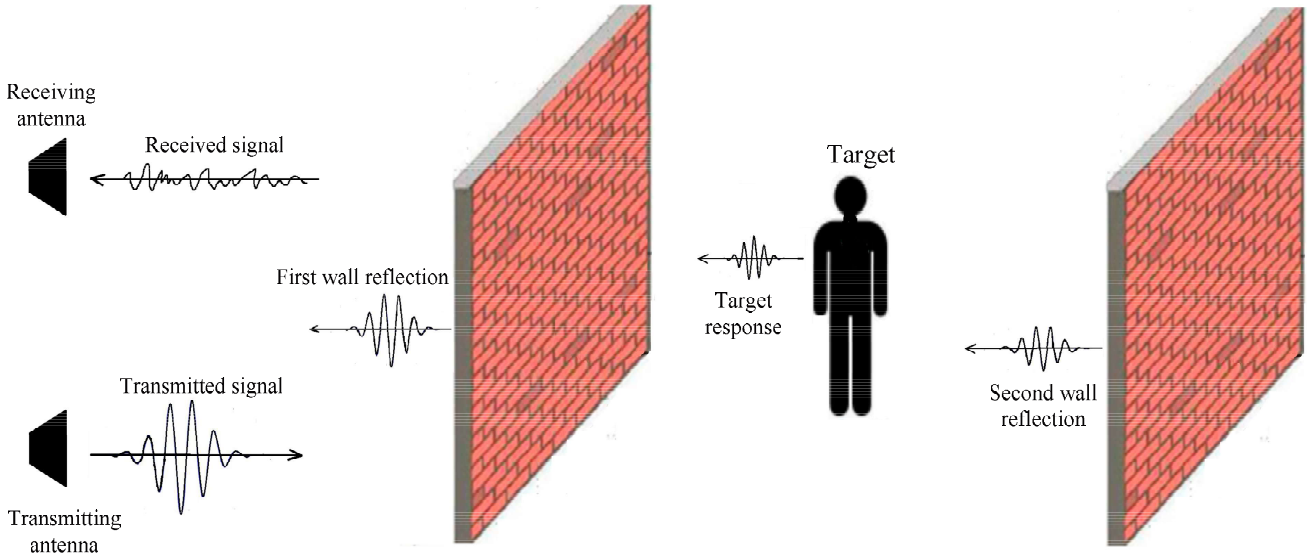
Figure 1. Through wall radar scenario.

walls around the target. Antenna self-reflection is the first part of the received signal which is produced because a part of the signal delivered to the antenna returns before transmission. Contrarily, the walls clutter appears later and overlaps with the target response. Figure 1 illustrates a through wall radar scenario and the corresponding signals.

A transmitted UWB Gaussian modulated sinusoidal pulse is given by [24]:

$$x\left(n\right) = e^{-\left(\frac{n}{\sigma}\right)^2} \cos\left(\omega_c n\right), \tag{1}$$

where σ is the pulse half-duration, n the discrete time index, and ω_c the carrier frequency. The radar received signal can be written as:

$$z\left(n\right) = \alpha_s x\left(n - \tau_s\right) + \sum_{i=1}^{k} \alpha_i x\left(n - \tau_i\right) + \alpha_T x\left(n - \tau_T\right), \tag{2}$$

where α_s is the antenna self-reflection factor, and α_i and α_T are the attenuation factors of the ith wall and the target, respectively. The factor τ_s is the time delay of the signal reflected back before the transmission; τ_i and τ_T are the time delays of the signals scattered by the ith wall and the target, respectively.

The first term in Eq. (2) represents the antenna return signal, while the second term is the summation of k walls reflections. The desired part in Eq. (2) is the third term which exemplifies the target response. The responsibility of a clutter removal technique is to eliminate or significantly mitigate the first two terms of Eq. (2) and preserves the target response.

Utilizing filters is one of the common approaches that have been used in clutter mitigation [21–23]. The core of the proposed algorithm is a filter described in detail in Section 3. Furthermore, the complete illustration of the proposed algorithm is presented in Section 4.

3. FILTER DESIGN

This section gives a full description for the filter adopted in the proposed algorithm. A filter with impulse response $h(n)$ can be used to filter out the unwanted parts from the signal $s(n)$ so that:

$$\tilde{y}\left(n\right) = h\left(n\right) * s\left(n\right), \tag{3}$$

where $\tilde{y}(n)$ represents the filtered signal.

In the frequency domain, Eq. (3) can be written as:

$$\tilde{Y}\left(w\right) = H\left(w\right) S\left(w\right). \tag{4}$$

The filter transfer function derivation is obtained by minimizing the mean square error between the original signal $y(n)$ and the filtered signal version $\tilde{y}(n)$ in the frequency domain as follows [25–27]:

$$
\begin{aligned}
\xi\left(w\right) &= E\left[\int |Y\left(w\right) - H\left(w\right) S\left(w\right)|^2 \, dw\right] \\
&= E\left[\int \left[Y\left(w\right) - H\left(w\right) S\left(w\right)\right]^* \left[Y\left(w\right) - H\left(w\right) S\left(w\right)\right] dw\right] \\
&= E\left[\int \left[Y^*\left(w\right) Y\left(w\right) - Y^*\left(w\right) H\left(w\right) S\left(w\right) - H^*\left(w\right) S^*\left(w\right) Y\left(w\right)\right.\right. \\
&\quad \left.\left. -H^*\left(w\right) S^*\left(w\right) H\left(w\right) S\left(w\right)\right] dw\right],
\end{aligned}
\tag{5}
$$

where $E[\cdot]$ is the expectation value, and $*$ represents a complex conjugate. Setting the mean square error derivative to zero:

$$
\begin{aligned}
0 &= \frac{\partial \xi\left(w\right)}{\partial H\left(w\right)} = E\left[-Y^*\left(w\right) S\left(w\right) - H^*\left(w\right) S^*\left(w\right) S\left(w\right)\right] \\
&= -\left[E\left[Y^*\left(w\right) S\left(w\right)\right] - E\left[|S\left(w\right)|^2\right] H^*\left(w\right)\right].
\end{aligned}
\tag{6}
$$

The original signal $S(w)$ contains both clean signal $Y(w)$ and the undesired signal $D(w)$, so:

$$
E\left[Y^*\left(w\right) S\left(w\right)\right] = E\left[Y^*\left(w\right)\left(Y\left(w\right) + D\left(w\right)\right)\right] = E\left[|Y\left(w\right)|^2\right].
\tag{7}
$$

Therefore, the optimum solution is [25–27]:

$$
H\left(w\right) = \frac{E\left[|Y\left(w\right)|^2\right]}{E\left[|S\left(w\right)|^2\right]} = \frac{E\left[|Y\left(w\right)|^2\right]}{E\left[|Y\left(w\right)|^2\right] + E\left[|D\left(w\right)|^2\right]}
\tag{8}
$$

where $E[|S(w)|^2]$ is obtained by averaging the signals in each frame of $|S(w)|^2$, and $E[|Y(w)|^2]$ can be estimated by spectral subtraction as $E[|S(w)|^2] - E[|D(w)|^2]$.

To make the filter $H(w)$ adaptive, $|\tilde{Y}(w)|$ is estimated iteratively:

$$
H_i\left(w\right) = \frac{\left|\tilde{Y}\left(w\right)_i\right|^2}{\left|\tilde{Y}\left(w\right)_i\right|^2 + E\left[|D\left(w\right)|^2\right]}
\tag{9}
$$

$$
Y\left(w\right)_{i+1} = H_i\left(w\right) S\left(w\right)
\tag{10}
$$

for $i = 0, 1, 2, \ldots$.

4. CLUTTER ELIMINATION PROCEDURE

The proposed algorithm includes multi-steps to remove the clutter from the monostatic radar signals and finally obtain a clutter mitigated image of an object behind the walls. Figure 2 depicts the entire proposed procedure, and the detailed demonstration of every step that is presented in this section.

First, the M radar received signals obtained from multiple A-scans of the zone in which the imaging is required are collected in a $N \times M$ matrix as follows:

$$
\mathbf{G} = \left[\begin{array}{cccc} \mathbf{z}_1 & \mathbf{z}_2 & \ldots & \mathbf{z}_M \end{array}\right]^T,
\tag{11}
$$

where $\mathbf{z}_i$ is the received signal at the ith antenna position, and N is the number of samples in each received signal.

In general, the clutter occurs at almost the same time in all the received radar monostatic signals, but the target response happens at different times due to the distance difference of the target with respect to each antenna. Thus, the proposed algorithm suggests dividing the time of processing as
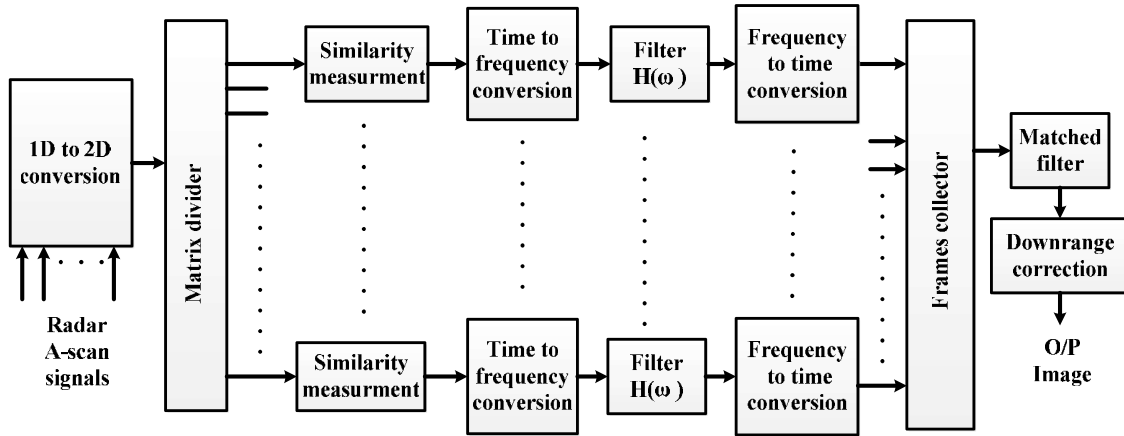
Figure 2. Block diagram of the proposed method.

individual frames. Matrix $\mathbf{G}$ is broken into P frame matrices $\mathbf{U}_1, \mathbf{U}_2, ..., \mathbf{U}_P$ with each of size $Q \times M$, such that $PQ = N$.

Next, the covariance of each frame matrix is found to measure the similarity between the received signals within each frame. The covariance is compared with a threshold value. Within each frame, if the covariance value is higher than the threshold value, the signals are synchronized, hence they are considered as a clutter frame matrix. Consequently, all the elements of clutter frame matrices are converted to a fixed value for improving the filtering process.

After that, the frame data are converted to frequency domain to be ready for filtering via $H(w)$. The filtering process is explained in detail in Section 3. The filter removes similar signals which represent the clutter, whilst it keeps the target response. The filtered data are returned to the time domain. Then, all the frame matrices are collected together to form matrix V of size $N \times M$. Now, the clutter in matrix V columns is eliminated. To enhance the target response, match filter is applied on each column of V.

Finally, the actual position of the target behind the walls is estimated. Because of the electromagnetic wave propagation speed difference in different media, the time of the reflected signals carries wrong information about the target downrange unless a distance correction is applied. The approach in [28] is used to estimate both the wall thickness and dielectric constant. The wall front side position in the B-scan image before the clutter elimination is very clear. The reflected signal time (T) is converted to downrange distance via the equation $d = vT/2$, where v is the speed of the electromagnetic wave in a medium having a dielectric constant ε_a, so that $v = c/\sqrt{\varepsilon_a}$, and c is the speed of light. The suggested downrange correction approach compresses the time of the reflected signals according to the estimated wall parameters. The signal samples between the time of front and rear wall reflections is down resampled by $\sqrt{\varepsilon_w}$ where ε_w is the estimated wall dielectric constant. Now, the processed radar signals are ready to be aligned in columns and displayed as a clutter eliminated, downrange corrected B-scan image.

5. SIMULATION AND RESULTS

To test the proposed algorithm in TWI clutter removal, the whole procedure is simulated in two parts: antenna design and applying TWI using radar in different scenarios. Then the radar raw data are processed using MATLAB to visualize the obtained images.

5.1. Antenna Design and Features

In radar TWI, the antenna is an essential tool that is used as a sensor to transmit and receive signals. UWB antennas are preferable to achieve high resolution in targets separation. Horn antenna has a simple design and a desirable radiation performance [29]. Hence, it is usually used in radar and microwave imaging [29]. To implement the simulation, a UWB horn antenna is designed using CST Microwave

Table 1. Designed antenna parameters.

Parameter	a	b	c	d	e	f	g
Length (mm)	51	12	9	23	52	36	5
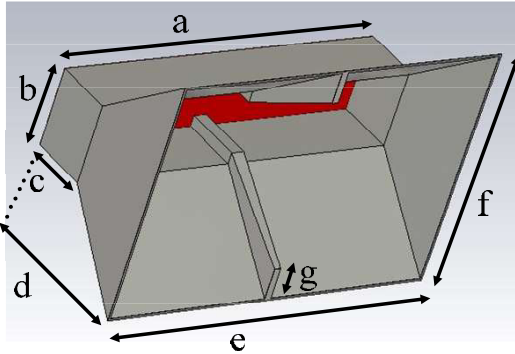
Figure 3. Designed UWB horn antenna.
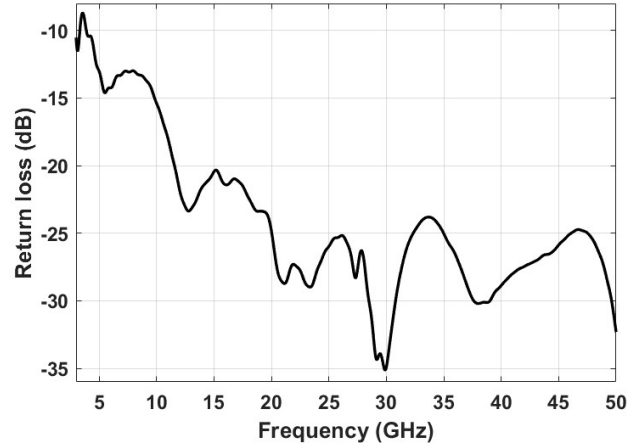
Figure 4. Designed UWB horn antenna S-parameter.
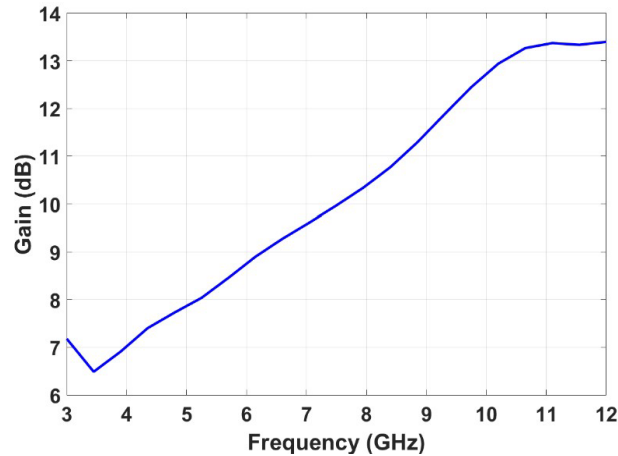
Figure 5. Antenna gain.

Studio software. Figure 3 shows the proposed UWB horn antenna configuration, while the antenna dimensions are listed in Table 1. Both the waveguide ridge thickness and height are 2 mm, and the ridge thickness at the horn aperture is 1 mm. In addition to the antenna compact design, the antenna covers a very high range of frequencies starting from 3.9 GHz. Figure 4 shows the antenna S_{11} parameter in the frequency range between 3 GHz and 50 GHz. The antenna gain versus the frequencies in the range between 3.9 GHz and 20 GHz is depicted in Figure 5, while the antenna far-fields at frequencies 4 GHz, 7 GHz, and 10 GHz are shown in Figure 6.

5.2. Clutter Removal Results

In this subsection, the effectiveness of the proposed algorithm in through wall radar clutter elimination is verified. Three different through wall scenarios are simulated using CST Microwave Studio software. The measurement is conducted using the designed horn antenna, and monostatic radar approach is
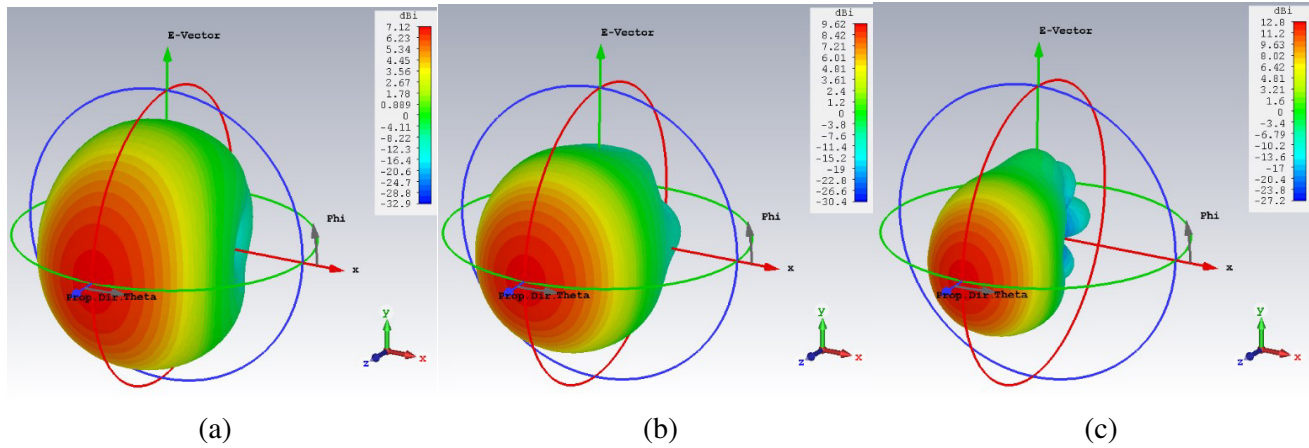
Figure 6. Antenna far-field: (a) at $4\,\text{GHz}$, (b) at $7\,\text{GHz}$, and (c) at $10\,\text{GHz}$.

adopted. The radar signal is a UWB Gaussian modulated sinusoidal signal with frequency band from $4\,\text{GHz}$ to $11\,\text{GHz}$. Through all the simulated environments, the wall thickness and relative permittivity are chosen to be $10\,\text{cm}$ and 4.5, respectively. The wall relative magnetic permeability is 1, while its conductivity is 0. The clutter in the filtered signals via the proposed algorithm is eliminated significantly. Thus, the resultant signals are ready to be used as input signals to any radar imaging algorithm. The performance of the proposed algorithm is evaluated using various criteria, such as TCR [13], SCR [30] which is the maximum target intensity to the maximum clutter intensity, and percentage value of DTPE. The criteria DTPE is defined as:

$$\text{DTPE} = \left| \frac{\text{actual downrange position} - \text{measured downrange position}}{\text{actual downrange position}} \right| * 100\% \tag{12}$$

The first scenario configuration, which is the simplest one, consists of the designed horn antenna, a brick wall, and a target as depicted in Figure 7. The target is a cylinder in z-direction and has an $11\,\text{cm}$ radius. The target is $66.6\,\text{cm}$ and $30\,\text{cm}$ far away in the z-direction from the antenna and the wall inner side, respectively. At each position, the antenna sends a UWB signal and collects the reflections using the monostatic radar approach. Then, the antenna is moved in a straight line with a step of $5\,\text{cm}$ on the x-direction. Thus, the scanning is repeated 25 times to cover the distance from $x = 0\,\text{cm}$ to $x = 120\,\text{cm}$. It is worth mentioning that the x-axis position of the target center is $72\,\text{cm}$.

Each of the 25 received signals has 6400 samples. As stated in Eq. (11), these signals are aligned vertically to form matrix **G**. This matrix represents the B-scan radar image and can be shown in
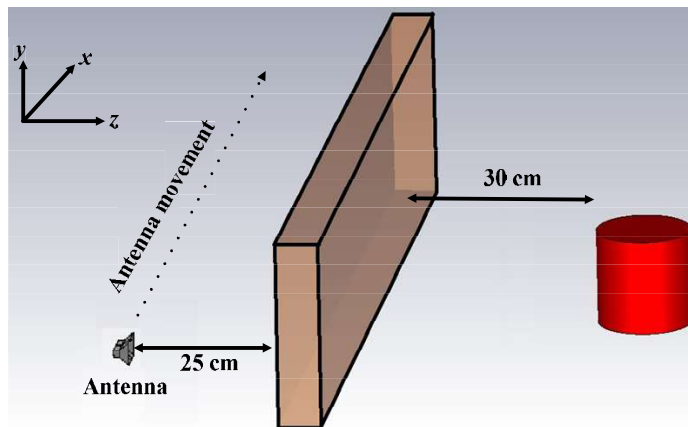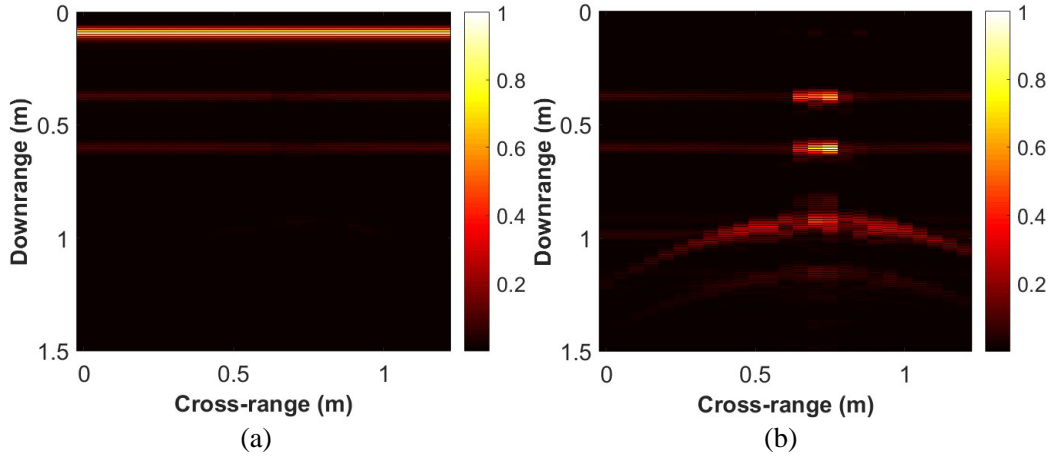

Figure 7. First scenario geometry.

Figure 8. B-scan images: (a) original, and (b) after averaging method.

Figure 8(a). Due to the bulkiness of the antenna self-reflection with respect to the other reflections, the return loss dominates the figure with weak air-wall and wall-air reflections. Moreover, the target reflection is missing in that image. The typical averaging method is applied on the formed matrix **G** to remove the clutter, and the obtained image is shown in Figure 8(b). Although the antenna self-reflection is removed, and the target response appears using the averaging method, this method does not eliminate the outer and inner wall reflections. In addition, a significant amount of clutter accompanies the target response in its position.

The proposed clutter elimination algorithm depends on the number of individual frames and the system threshold value. To test the effect of the frames number on the algorithm performance, matrix **G** is divided into different frames; 5, 10, 20, and 40 frames, then the algorithm is applied. Figure 9 shows the obtained B-scan image after data processing with these frame numbers. It can be noticed that dividing **G** into 20 frames produces the best result. Thus, this value is considered for all the tests in this work.

To select the optimal threshold value, the covariance is computed for the signals in each frame, and covariance values versus the frames index are plotted in Figure 10. The high covariance values at the early time of this figure represent the high similarity of antenna return loss and wall reflections, while the low covariance values at late time exemplify the target response. Based on the covariance values, the threshold value is selected. In this scenario, all the low values are less than 0.3; therefore, this value is adopted as the threshold value.

After removing the clutter from the B-scan radar image, the target downrange needs to be corrected. Figures 11(a) and 11(b) depict the images before and after downrange correction, respectively. Although the cross-range of the target is accurate which is at $x = 72$ cm in Figure 11(a), the downrange is wrong because of the wall effect. The correct downrange starts at $z = 65$ cm, whilst it appears at $z = 81.7$ cm. The downrange is corrected according to the procedure described in Section 4. The position of the wall front side is obtained from the original image in Figure 8(a). The estimated wall thickness and dielectric constant are 10.2 cm and 4.7, respectively. The resulting image after the downrange correction is shown in Figure 11(a). The target downrange in this figure starts at $z = 64.8$ cm which is very close to the right range. The TCR, SCR, and DTPE of the first scenario before and after applying the proposed algorithm are listed in Table 2. The proposed algorithm fulfills a significant improvement in all the measured criteria. For TCR and SCR, the enhancement values are 48.1 dB and 57.4 dB, respectively. The error in the downrange decreases from 25.6% to 0.3%.

To test the performance of the proposed algorithm in removing clutter in the presence of multiple closely spaced targets, two targets are simulated behind the wall described in the first scenario at the same downrange which is 65 cm. Each target is a cylinder having a radius of 10 cm. The distance between the targets is 18 cm. The cross-ranges of the targets are 44 cm and 82 cm. Figures 12(a) and 12(b) show the two targets B-scan images before and after removing the clutter by using the proposed algorithm,
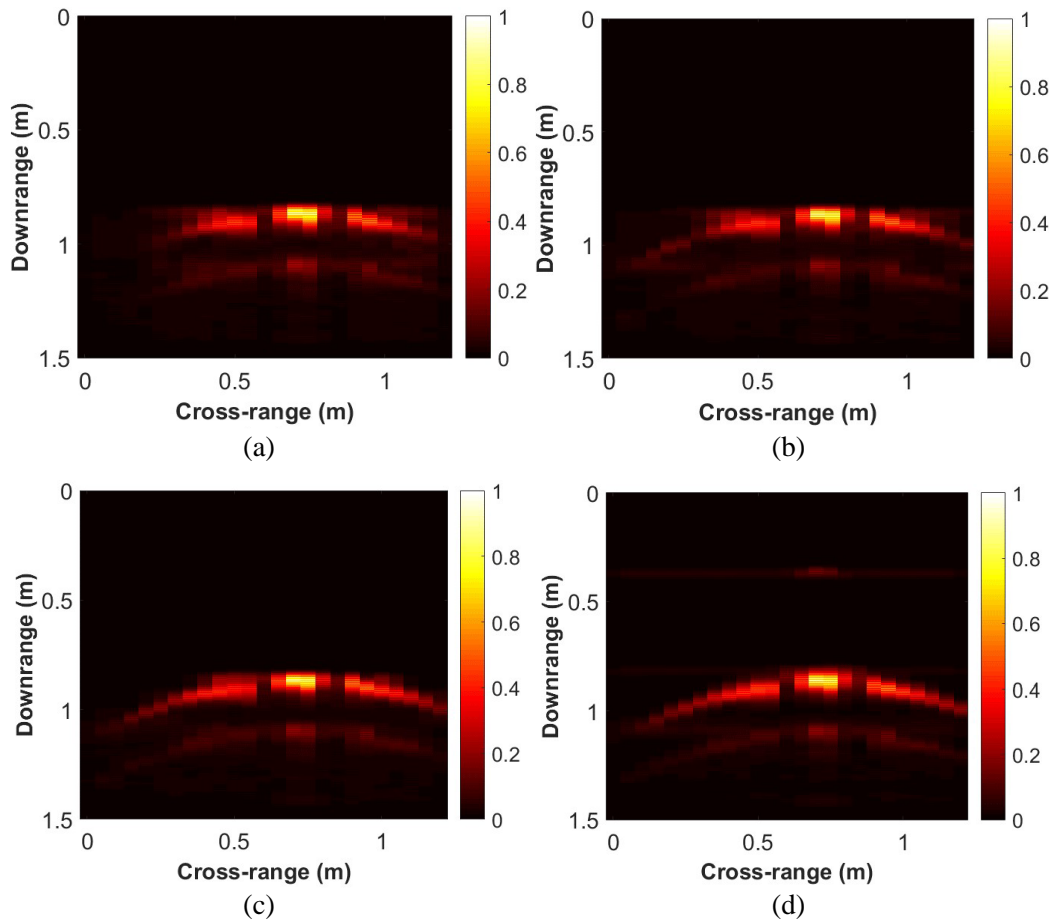
Figure 9. B-scan images after applying the proposed method with different frames: (a) five frames, (b) ten frames, (c) twenty frames and (d) forty frames.
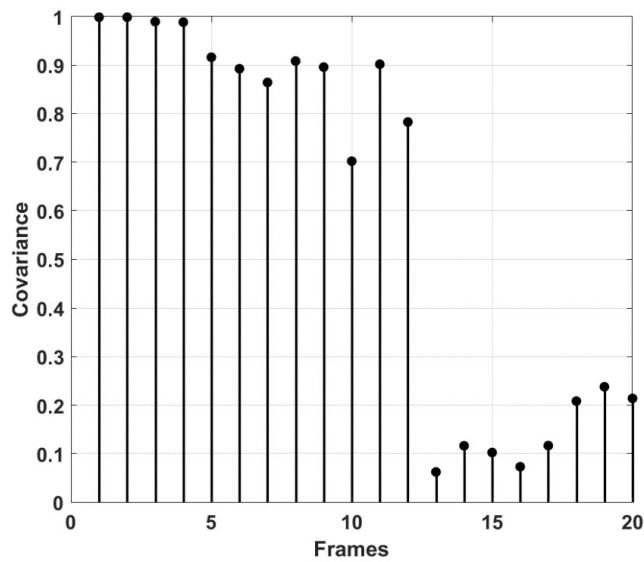

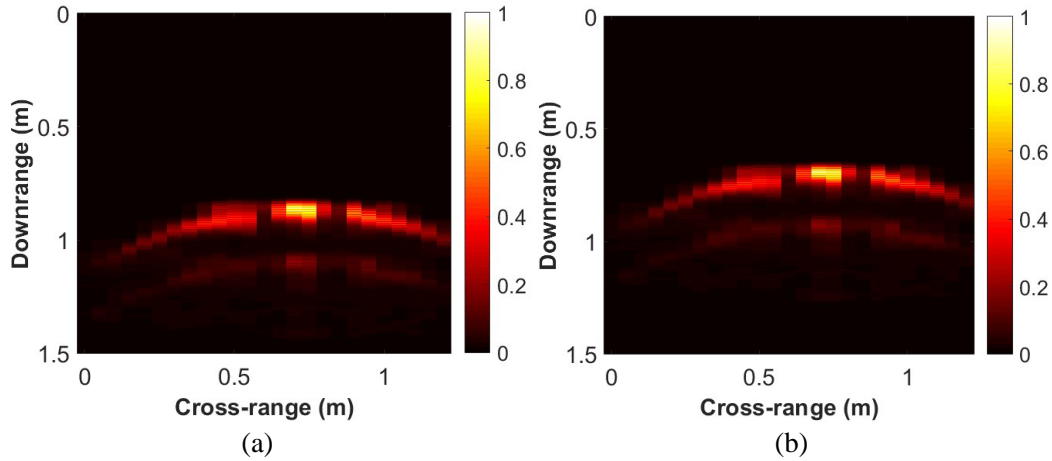**Figure 10.** Signals covariance in each frames.

Figure 11. B-scan images after applying the proposed method with 20 frames: (a) before downrange correction and (b) after downrange correction.
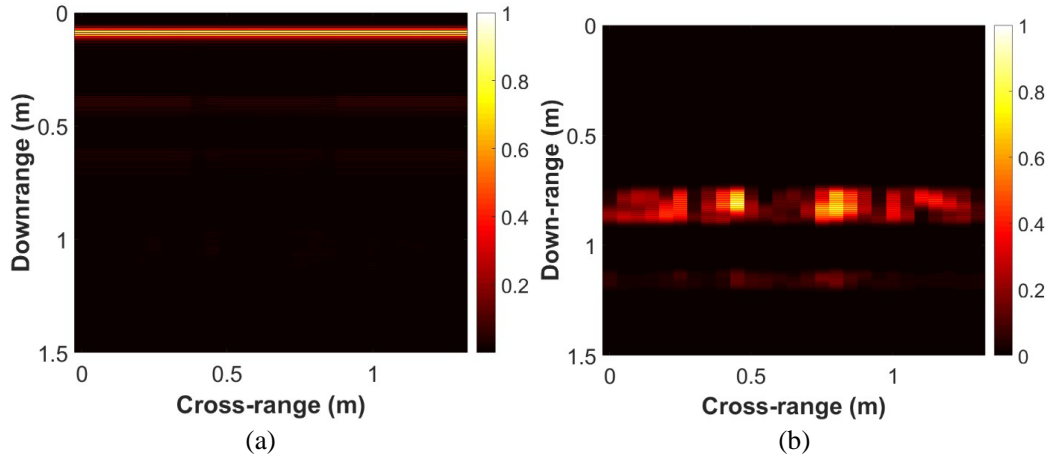

Figure 12. Two targets B-scan images: (a) original and (b) after applying the proposed algorithm.

respectively. Both of the targets are missing in the radar image before the clutter removing due to the dominance of the antenna self-reflection. Conversely, the proposed algorithm significantly removes the clutter and successfully discriminates the two targets at their corresponding cross-ranges.

The second scenario is similar to the first one except that the target is between two walls as shown in Figure 13, which complicates the situation by adding more reflections and consequently additional clutter. The distance between the walls is $100\,\mathrm{cm}$, whereas the target is $60\,\mathrm{cm}$ behind the first wall. The scanning way is achieved in the same manner as that in the first scenario. The antenna movement in the x-direction stars from $x = 0$ to $x = 110\,\mathrm{cm}$. The target is also a cylinder with the same radius and material of the first scenario target. The target position corresponding to the $x-$axis coordinate in this scenario is $40\,\mathrm{cm}$.

Figure 14(a) illustrates the second scenario B-scan image resulting from collecting the radar A-scan data without any processing. The antenna self-reflection and the first wall reflections appear only in this figure; the target and the second wall are absent because their responses are weak. In Figure 14(b), the averaging method is applied to remove the clutter. Although the antenna reflection is removed by using this method, the target is hardly recognizable in the image. Furthermore, the wall clutter is strongly widespread and dominant. Figure 14(c) illustrates the second scenario B-scan image after eliminating the clutter and correcting the downrange by the proposed algorithm. The clutter is
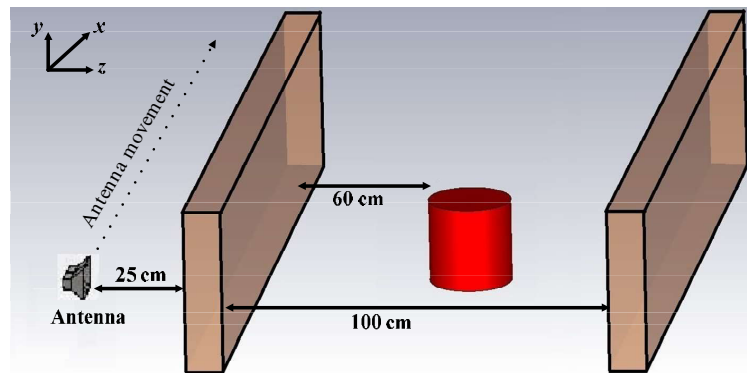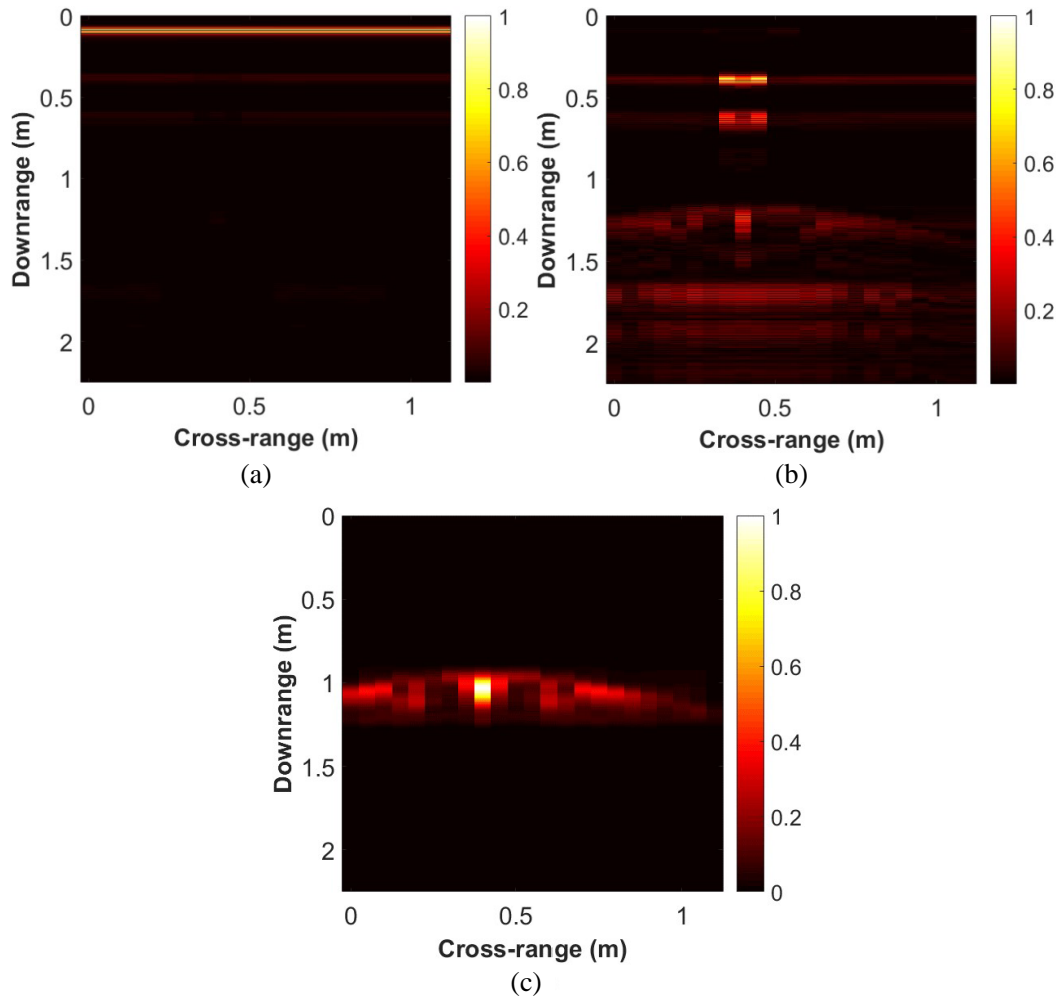
Figure 13. Second scenario geometry.

Figure 14. B-scan images: (a) original, (b) after averaging method and (c) after applying the proposed algorithm.

significantly removed, and the target is clearly visible in this figure. The target is detected accurately with cross-range and downrange of 40 cm and 93 cm, respectively. Thus, the error in the detected cross-range is 0 cm, with only 2 cm shift in the downrange estimation. Table 2 lists the improvement in TCR,

Table 2. The proposed algorithm performance.

Scenario		TCR (dB)	SCR (dB)	DTPE (%)
First	Before the proposed processing	−3.9	−28.3	25.6
	After the proposed processing	44.2	29.1	0.3
Second	Before the proposed processing	−2.3	−30.4	9.5
	After the proposed processing	34.7	33.9	2.1
Third	Before the proposed processing	−11.1	−40.3	10.5
	After the proposed processing	39.6	30.4	2.9

SCR, and DTPE measurement parameters by using the proposed algorithm. These parameters indicate 36.9 dB, 46.3 dB, 7.4% amelioration for TCR, SCR, and DTPE, respectively.

The clutter elimination efficiency of the proposed algorithm is examined in a more complicated scenario where two walls are placed in the space between the antenna and the target as illustrated in Figure 15. The distance of the hall between the walls is 75 cm, whereas the distance between the second wall and the target is 50 cm. Therefore, the whole distance between the antenna and the target is 170 cm. The target is a semi-cylinder of an 11 cm radius and located at a cross-range of 80 cm. The radar scanning is achieved by moving the antenna with a step of 10 cm from $x = 0$ cm to $x = 160$ cm. As a result of two walls existence with a hall separating them, the electromagnetic wave transmitting in the z-direction suffers from several reflections and scattering which lead to producing more clutter in the B-scan image.
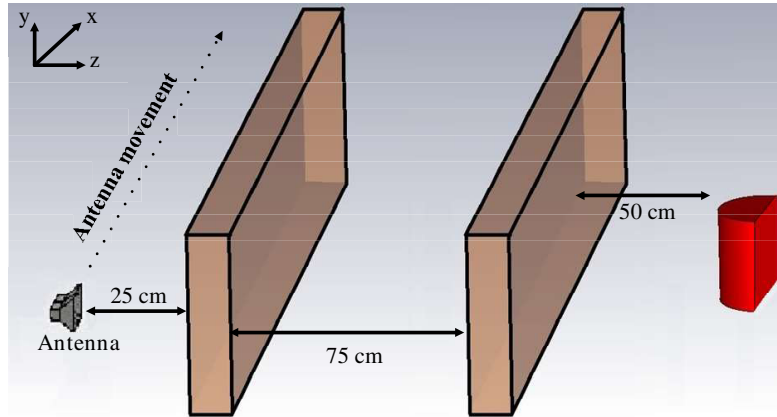
Figure 15. Third scenario geometry.

The A-scan radar signals are aligned vertically without processing, and the B-scan image is depicted in Figure 16(a). The objects appearing in that figures from top to bottom are: the antenna reflection, the front and back of the first wall, and the front and back of the second wall. The absence of the target is clear in that image. After averaging processing as shown in Figure 16(b), the target records a slight presence compared to the governing clutter. On the other hand, the B-scan image in Figure 16(c) shows the superiority of the proposed algorithm in removing the clutter and showing the target powerfully. Moreover, this figure shows the capability of the proposed algorithm in estimating the target downrange accurately. The third scenario performance evaluation criteria shown in Table 2 record 49.7 dB, 70.7 dB, and 7.6% for TCR, SCR, and DTPE, respectively.

Figure 17 illustrates the effectiveness of the proposed algorithm in clutter removing and downrange adjusting. One of the A-scan radar signals is shown in Figure 17(a) where the antenna and walls high
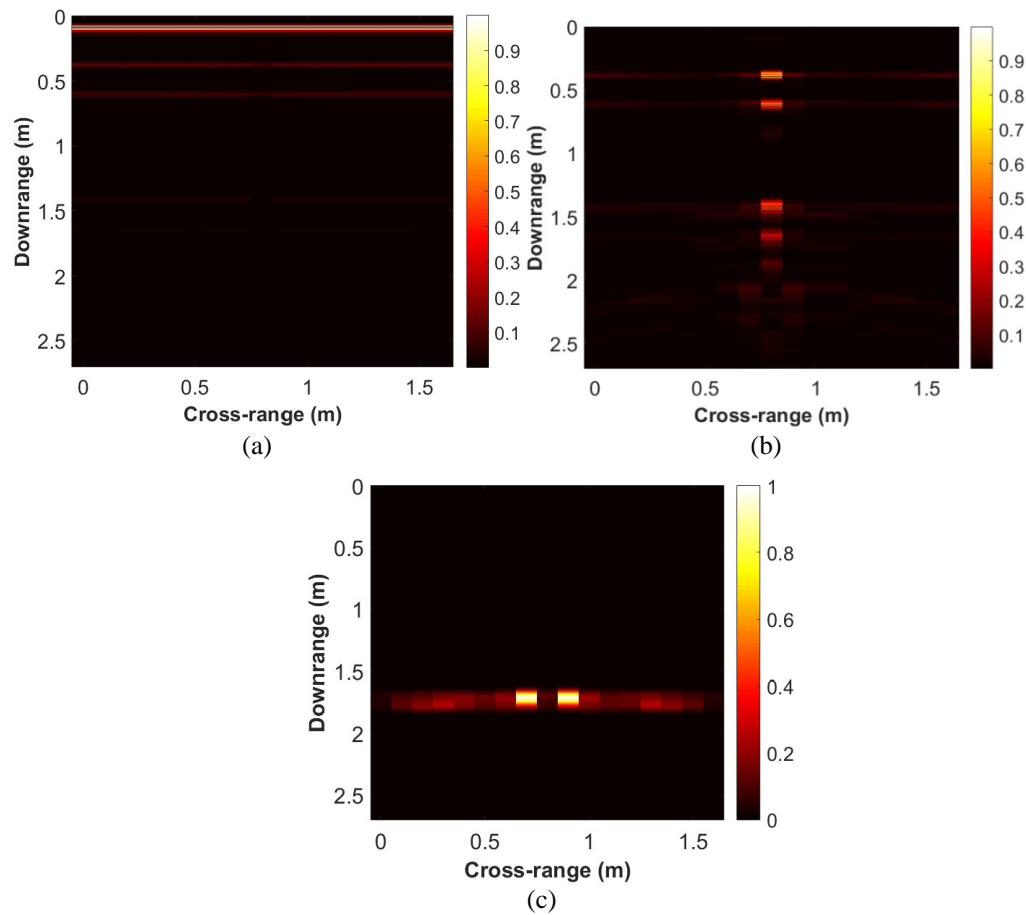
Figure 16. B-scan images: (a) original, (b) after averaging method and (c) after applying the proposed algorithm.
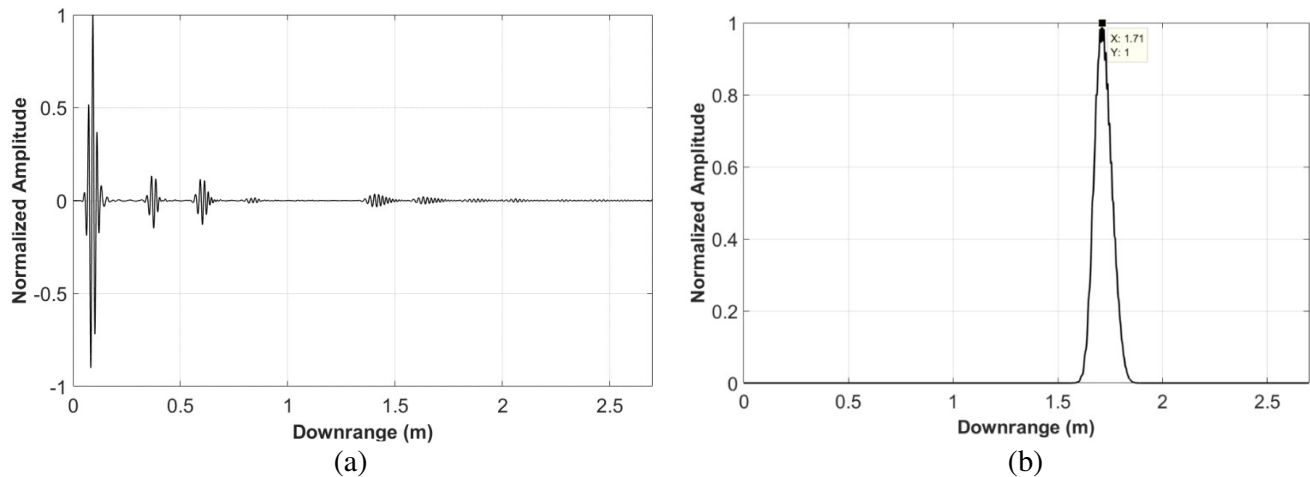

Figure 17. Radar received signal: (a) before processing and (b) after processing.

reflections produce clutter which veil the target response in the B-scan image. After the processing with the proposed algorithm, the clutter is significantly removed, and the target is successfully detected with an accurate downrange as shown in Figure 17(b).

For various through wall scenarios, the proposed algorithm dazzlingly succeeds in removing clutter from obtained through wall B-scan images. In addition, the target downrange is accurately corrected via the proposed algorithm which highlights it as a well-qualified candidate to be adopted for through wall radar clutter removal.

Finally, the performance of the proposed algorithm is compared with some clutter removal techniques which have been mentioned in the introduction section. The techniques included in the comparison are the averaging, MAW, and ICA. The comparison results are listed in Table 3. For all the scenarios, the proposed algorithm remarkably overcomes the other techniques in all the tested objective metrics. Generally, the performance arrangement can be sorted from the best to the worst as: the proposed algorithm, ICA, then MAW and averaging which show close results.

Table 3. Performance comparison.

Scenario	Method	TCR (dB)	SCR (dB)	DTPE (%)
First	Averaging	29.8	5.5	23
	MAW	30.6	4.5	23
	ICA	36.5	20.7	33
	Proposed	44.2	29.1	0.3
Second	Averaging	21.7	-0.14	21
	MAW	20.7	-0.34	19.6
	ICA	32.8	13.4	20
	Proposed	34.7	33.9	2.1
Third	Averaging	17	-3.3	17.6
	MAW	17.1	-2.1	17
	ICA	27.9	9.1	13.4
	Proposed	39.6	30.4	2.9

6. CONCLUSION

The proposed algorithm in this paper can significantly remove the clutter from the radar signals in radar through wall detection. The antenna and walls reflections, which cause clutter, happen at a fixed time in all the monostatic radar signals, while the target response is received at different times according to the target position with respect to antenna scanning location. Thus, dividing the data in time and exploiting the clutter similarity in each divided signal part is useful in filtering the clutter and preserving the target reflection. Three different scenarios are used to evaluate the performance of the proposed algorithm. The three scenarios are a target behind a wall, a target between two walls, and a target behind two separated walls. The proposed algorithm well removes the clutter in all these scenarios. Applying the proposed algorithm improves the TCR by 48.1 dB, 37 dB, and 49.7 dB for the first, second, and third scenarios, respectively. The improvements in SCR are 57.3 dB, 64.3 dB, and 70.7 dB for the corresponding scenarios. In addition to the clutter removing, the proposed algorithm can correct the target downrange error caused by signal diffraction and speed change of the electromagnetic waves through the walls. Without utilizing the proposed algorithm, the DTPE reaches 25.6% in one of the simulated scenarios, whilst the maximum DTPE is only 2.9% after applying the proposed algorithm. Finally, the performance comparison of the proposed technique with some common techniques verifies the excellence of the proposed technique over the others in both clutter elimination and downrange correction.

REFERENCES

1. Baharian, M., H. Rajabalipanah, M. H. Fakheri, and A. Abdolali, "Removing the wall effects using electromagnetic complex coating layer for ultra-wideband through wall imaging," *IET Microwaves, Antennas & Propagation*, Vol. 11, No. 4, 477–482, 2017.

2. Thajudeen, C. and A. Hoorfar, "A hybrid bistatic-monostatic radar technique for calibration-free estimation of lossy wall parameters," *IEEE Antennas & Wireless Propagation Letters*, Vol. 16, 1249–1252, 2017.

3. Vishwakarma, S. and S. S. Ram, "Mitigation of through-wall distortions of frontal radar images using denoising autoencoders," *IEEE Transactions on Geoscience & Remote Sensing*, Vol. 58, No. 9, 6650–6663, Sept. 2020.

4. Zhu, Z., D. Yang, J. Zhang, and F. Tong, "Dataset of human motion status using IR-UWB through-wall radar," *Journal of Systems Engineering & Electronics*, Vol. 32, No. 5, 1083–1096, Oct. 2021.

5. Liu, X., H. Leung, and G. A. Lampropoulos, "Effect of wall parameters on ultra-wideband synthetic aperture through-the-wall radar imaging," *IEEE Transactions on Aerospace & Electronic Systems*, Vol. 48, No. 4, 3435–3449, Oct. 2012.

6. Al-Zuhairi, D. T., A. M. Abed, J. M. Gahl, and N. E. Islam, "Phase-based window function and CD-DMAS beamforming for microwave breast cancer detection," *IET Microwaves, Antennas & Propagation*, Vol. 14, No. 7, 608–616, 2020.

7. Dong, Z., B. Xue, J. Lei, X. Zhao, and J. Gao, "Study on propagation characteristics of ground penetrating radar wave in dikes and dams with polymer grouting repair using finite-difference time-domain with perfectly matched layer boundary condition," *Sustainability*, Vol. 14, No. 16, 1–15, 2022.

8. Tivive, F. H. C., A. Bouzerdoum, and M. G. Amin, "A subspace projection approach for wall clutter mitigation in through-the-wall radar imaging," *IEEE Transactions on Geoscience & Remote Sensing*, Vol. 53, No. 4, 2108–2122, Apr. 2015.

9. Zhang, L. Z., B. Y. Lu, Z.-M. Zhou, and X. Sun, "A wall-clutter suppression method based on spatial signature in MIMO through-the-wall radar imaging," *Progress In Electromagnetics Research B*, Vol. 55, 277–295, 2013.

10. Sleasman, T., M. F. Imani, M. Boyarsky, K. P. Trofatter, and D. R. Smith, "Computational through-wall imaging using adynamic metasurface antenna," *OSA Continuum*, Vol. 2, No. 12, 3499–3513, Dec. 2019.

11. Lazaro, A., D. Girbau, and R. Villarino, "Techniques for clutter suppression in the presence of body movements during the detection of respiratory activity through UWB radars," *Sensors*, Vol. 14, No. 2, 2595–2618, 2014.

12. Verma, P. K., A. N. Gaikwad, D. Singh, and M. J. Nigam, "Analysis of clutter reduction techniques for through wall imaging in UWB range," *Progress In Electromagnetics Research B*, Vol. 17, 29–48, 2009.

13. Lim, Y. and S. Nam, "Target-to-clutter ratio enhancement of images in through-the-wall radar using a radiation pattern-based delayed-sum algorithm," *Journal of Electromagnetic Engineering & Science*, Vol. 14, No. 4, 405–410, Dec. 2014.

14. Zheng, C., X. Xi, and Z. Song, "Through-the-wall radar clutter mitigation using stepped-frequency signal," *Electronics Letters*, Vol. 55, No. 1, 53–55, 2018.

15. Zhang, Y. and T. Xia, "In-wall clutter suppression based on low-rank and sparse representation for through-the-wall radar," *IEEE Geoscience & Remote Sensing Letters*, Vol. 13, No. 5, 671–675, May 2016.

16. Tang, V. H., A. Bouzerdoum, and S. L. Phung, "Wall clutter mitigation for radar imaging of indoor targets: A matrix completion approach," *21st Asia Pacific Symposium on Intelligent and Evolutionary Systems (IES)*, 116–121, Hanoi, Vietnam, 2017.

17. Tivive, F. H. C. and A. Bouzerdoum, "Clutter removal in through-the-wall radar imaging using sparse autoencoder with low-rank projection," *IEEE Transactions on Geoscience & Remote Sensing*, Vol. 59, No. 2, 1118–1129, Feb. 2021.

18. Zhou, Y., C. Huang, H. Liu, D. Li, and T.-K. Truong, "Front-wall clutter removal in through-the-wall radar based on weighted nuclear norm minimization," *IEEE Geoscience & Remote Sensing Letters*, Vol. 19, No. 3501405, 1–5, Nov. 2022.

19. Vishwakarma, S. and S. S. Ram, "Mitigation of through-wall distortions of frontal radar images using denoising autoencoders," *IEEE Transactions on Geoscience & Remote Sensing*, Vol. 58, No. 9, 6650–6663, Sept. 2020.

20. Shi, X., C. Wang, and C. Zheng, "Wall clutter mitigation based on spread spectrum radar in through-the-wall radar," *Microwave and Optical Technology Letters*, Vol. 62, No. 5, 1987–1990, May 2020.

21. Yoon, Y.-S. and M. G. Amin, "Spatial filtering for wall-clutter mitigation in through-the-wall radar imaging," *IEEE Transactions on Geoscience & Remote Sensing*, Vol. 47, No. 9, 3192–3208, Sept. 2009.

22. Kim, B., D. Kim, Y. Lim, D. Yang, S. Nam, and J.-H. Song, "A clutter rejection technique using a delay-line for wall-penetrating FMCW radar," *IEICE Transactions on Electronics*, Vol. 99-C, No. 5, 597–600, 2016.

23. Yang, S., H. Qin, X. Liang, and T. A. Gulliver, "Clutter elimination and harmonic suppression of non-stationary life signs for long-range and through-wall human subject detection using Spectral Kurtosis Analysis (SKA)-based Windowed Fourier Transform (WFT) method," *Applied Sciences*, Vol. 9, No. 2, 2019.

24. Banerjee, P. P. and G. Nehmetallah, "Linear and nonlinear propagation in negative index materials," *Journal of the Optical Society of America B*, Vol. 23, No. 11, 2348–2355, Nov. 2006.

25. Loizou, P. C., *Speech Enhancement Theory and Practice*, 2nd Edition, CRC Press, Taylor & Francis Group, NW Boca Raton, FL, USA, 2013.

26. Jaiswal, R. and D. Romero, "Implicit wiener filtering for speech enhancement in non-stationary noise," *11th International Conference on Information Science & Technology (ICIST)*, 39–47, Chengdu, China, May 21–23, 2021.

27. Jaiswal, R. K., S. R. Yeduri, and L. R. Cenkeramaddi, "Single-channel speech enhancement using implicit Wiener filter for high-quality speech communication," *International Journal of Speech Technology*, Vol. 25, No. 3, 745–758, 2022.

28. Aftanas, M., J Sachs, M. Drutarovský, and D. Kocur, "Efficient and fast method of wall parameter estimation by using UWB radar system," *Frequenz*, Vol. 63, Nos. 11–12, 231–235, 2009.

29. Al-Zuhairi, D. T., J. M. Gahl, and N. E. Islam, "Compact dual-polarized quad-ridged UWB horn antenna design for breast imaging," *Progress In Electromagnetics Research C*, Vol. 72, 133–140, 2017.

30. Liu, L., Q. Chen, Y. Han, H. Xu, J. Li, and B. Wang, "Improved clutter removal by robust principal component analysis for chaos through-wall imaging radar," *Electronics*, Vol. 9, No. 25, 2020.